SCIENTIA
IRANICA

Estimation of Stress Drop for Some Large Shallow Earthquakes Using Stochastic Point Source and Finite Fault Modeling

H. Moghaddam[1], N. Fanaie[2,*] and D. Motazedian[3]

Abstract. *Using stochastic point source and finite fault modeling, the stochastic stress drop is estimated for 52 large shallow earthquakes listed in the 'Pacific Earthquake Engineering Research Center (PEER) Next Generation Attenuation of Ground Motions (NGA)' database. The Pseudo Spectral Acceleration (PSA) of 541 accelerograms, recorded at National Earthquake Hazards Reduction Program (NEHRP) C-class sites from 52 earthquakes are simulated and compared with the PSA listed in the PEER NGA database. The magnitude of the analyzed earthquakes ranged from M 4.4 to M 7.6. The stress drop is calibrated by trial and error and based on the analysis of residuals where the residual is defined as the log of the observed PSA minus the log of the predicted PSA by stochastic methods. The symmetric distribution of residuals around the zero line is considered as an indicator of good agreement between the simulated and observed PSAs. The calculated stress drops based on stochastic point source and finite fault modeling are different from the static stress drops that are currently listed in the PEER NGA database. It seems that there is no clear relation between stress drop and earthquake magnitude, but there is a good linear relation between estimated stress drops based on stochastic point source and finite fault modeling. The sensitivity of the estimated stress drop values on the Kappa factor and geometric speeding factor (b value) is also investigated.*

Keywords: *Large shallow earthquakes; Stress drop; Stochastic point source modeling; Stochastic finite fault modeling.*

INTRODUCTION

Earthquake simulation is a powerful tool in earthquake engineering and engineering seismology. In this research, stochastic point source and finite fault modeling are used to simulate the acceleration time series for large shallow earthquakes listed in the PEER NGA database. One of the main input parameters in stochastic simulation methods is stress drop, which controls the levels of the spectrum at high frequencies being usually more than 1 Hz.

The purpose of this article is to apply stochastic point source and finite fault modeling, estimate the average stress drops for the PEER NGA database and compare them with the current static stress drops currently given in that database. These results can be used in future application of stochastic methods in cases where there is no information on the stress drop value. Using stochastic finite fault modeling to estimate the stress drop has been done for different regions [1-5].

There are three commonly used approaches in stochastic modeling:

i)   Point source with a single corner, ω^2, source spectrum [6,7].

ii) Point source with a two-corner source spectrum [8,9].

iii) Finite fault approaches [2,3,10-14].

The first method, point source modeling, has been widely used and provides good results for small to moderate earthquakes, but it overestimates lower fre-

---

1. *Department of Civil Engineering, Sharif University of Technology, Tehran, P.O. Box 11155/8639, Iran.*
2. *Department of Civil Engineering, Khajeh Nasirodin Toosi University of Technology, Tehran, P.O. Box 15875/4416, Iran.*
3. *Carleton University, Ottawa, Ontario, K1S 5B6, Canada.*
*. *Corresponding author. E-mail: nader_fanaie@kntu.ac.ir*

quencies for larger earthquakes [15]. The effects of a large earthquake fault including fault geometry, heterogeneity of slip on the fault plane and directivity can influence the amplitudes, frequency content and duration of the ground motion.

To overcome the overestimation of low frequencies by stochastic point source modeling, the second method, which is point source modeling with a two-corner source, was introduced to model finite fault effects on ground motion radiation [8,9]. However, the two-corner frequency model is directly independent of the stress drop; the input parameter that we are interested in for this study.

The third method, finite fault modeling using both stochastic and other approaches, has been an important tool for the prediction of near-source ground motion of large earthquakes [1,2,10-13,16-21]. In this article, both stochastic point source [6] and finite fault modeling based on a dynamic corner frequency [3] are applied using the EXSIM (EXtended fault SIMulation) program for ground motion simulation.

DATABASE

In this study, the response spectra of 541 horizontal-component time series recorded at NEHRP C-class sites from the PEER NGA database were analyzed. The NEHRP C-class site (rock site) was chosen to minimize the effects of site response and *Kappa* factor (rapid spectral decay at high frequencies) in the calibration of stress drop. These records are from 52 large shallow earthquakes that occurred all over the world. Since the geometric spreading factor (b value − see Equation 1) is also a very important factor in the simulation of far-field earthquakes, the maximum distance of 60 km was chosen to minimize the post-critical reflection effects from Moho discontinuity. The studied earthquakes are presented in Table 1. Five abbreviations are used in Table 1 for different types of earthquake: SS for strike slip, N for normal, R for reverse, RO for reverse oblique and NO for normal oblique.

STOCHASTIC MODELING

Point Source Modeling Approach

Stochastic point source modeling is a widely used tool for the simulation of acceleration time series. The goal of this method is the generation of a transient time series that has a stochastic character and where the spectrum matches a specified desired amplitude [6,22]. First, a window is applied to a time series of Gaussian noise with zero mean and unit variance. The windowed time series is transformed to the frequency domain, and the amplitude spectrum of the random time series is

multiplied by the desired spectrum. Transformation back to the time domain results in a stochastic time series, where the amplitude spectrum is the same, on average, as the desired spectrum. The application of this method clearly requires specification of the target amplitude spectrum of the earthquake to be simulated; therefore, the stochastic method needs a model that specifies the Fourier spectrum of ground motion as a function of magnitude and distance. Often, the acceleration spectrum is modeled by a spectrum with a ω^2 shape, where ω is the angular frequency [6,23,24]. The acceleration spectrum of the shear waves, $A(f)$, at hypocentral distance, R, from an earthquake is given by:

$$A(f) = (CM_0(2\pi f)^2/[1 + (f/f_0)^2])$$

$$\exp(-\pi f R/Q\beta)\exp(-\pi f\kappa)D(f)/R^b, \quad (1)$$

where M_0 is seismic moment and f_0 is corner frequency, which is given by $f_0 = 4.9 * 10^6 \beta (\Delta\sigma/M_0)^{1/3}$, where $\Delta\sigma$ is stress drop in bars, M_0 is in dyne-cm and β is shear wave velocity in km/s. Constant $C = \Re^{\theta\varphi}FV/(4\pi\rho\beta^3)$, where $\Re^{\theta\varphi}$ is the radiation pattern (average value of 0.55 for shear waves), F is the free surface amplification (2.0), V is the partition into two horizontal components (0.71), ρ is the density and R is the hypocentral distance [6]. The term $\exp(-\pi f\kappa)$ is a high cut filter to model zero distance *Kappa* effects, which are commonly observed rapid spectral decays at high frequencies [25]. The quality factor, $Q(f)$, is inversely related to anelastic attenuation. The term, $1/R^b$, shows geometrical spreading. If $b = 1$, the term of $1/R$ is appropriate for body wave spreading in a whole space. $1/R$ can be changed as needed, in order to account for the presence of the post-critical reflections from Moho discontinuity. $D(f)$ is the site amplification term, which is a function of frequency and depends on soil type. It should be noted that in this model the spectrum is derived for an instantaneous shear dislocation at a point.

Finite Fault Modeling Approach

To extend point source modeling to finite fault modeling, a large fault is divided into N subfaults, and each subfault is considered as a point source [16]. In this model, the rupture spreads radially from the hypocenter. The ground motion of each subfault is calculated by stochastic point source modeling. The ground motions of subfaults are then summed in the time domain with a proper delay time, which depends on the distance between each subfault and the observation point.

There are different programs for stochastic finite fault modeling; and, in this research, we used the

Table 1. PEER NGA database earthquakes recorded at NEHRP C-class sites (continued).

Earthquake Name	Date	Magnitude	# of NEHRP C Records	Quality Factor
Parkfield[SS]	1966/06/28	6.2	2	[1]$180f^{0.45}$
Coyote Lake[SS]	1979/08/06	5.7	5	$180f^{0.45}$
Livermore-01[SS]	1980/01/24	5.8	2	$180f^{0.45}$
Livermore-02[SS]	1980/01/27	5.8	3	$180f^{0.45}$
Anza (Horse Canyon)-01[SS]	1980/02/25	5.6	3	$180f^{0.45}$
Mammoth Lakes-02[SS]	1980/05/25	6.0	1	$180f^{0.45}$
Mammoth Lakes-08[SS]	1980/05/31	4.9	2	$180f^{0.45}$
Westmorland[SS]	1981/04/26	5.9	1	$180f^{0.45}$
Morgan Hill[SS]	1984/04/24	6.1	9	$180f^{0.45}$
Hollister-04[SS]	1986/01/26	5.4	1	$180f^{0.45}$
Superstition Hills-02[SS]	1987/11/24	6.5	1	$180f^{0.45}$
Landers[SS]	1992/06/28	7.3	4	$180f^{0.45}$
Big Bear-01[SS]	1992/06/28	6.5	2	$180f^{0.45}$
Hector Mine[SS]	1999/10/16	7.1	2	$180f^{0.45}$
Yountville[SS]	2000/09/03	5.2	3	$180f^{0.45}$
Big Bear-02[SS]	2001/02/10	5.3	9	$180f^{0.45}$
Gilroy[SS]	2002/05/14	5.2	7	$180f^{0.45}$
Chi-Chi, Taiwan-04[SS]	1999/09/20	6.4	1	[2]$117f^{0.77}$
Oroville-02[N]	1975/08/02	4.8	2	$180f^{0.45}$
Oroville-03[N]	1975/08/08	4.7	8	$180f^{0.45}$
Irpinia, Italy-01[N]	1980/11/23	6.9	3	[3]$130f^{0.1}$
Irpinia, Italy-02[N]	1980/11/23	6.2	2	$130f^{0.1}$
Lazio-Abruzzo, Italy[N]	1984/05/07	5.9	1	$130f^{0.1}$
Kozani, Greece-01[N]	1995/05/13	6.5	1	[4]$85f^{0.91}$
Little Skull Mtn, NV[N]	1992/06/29	5.7	1	$180f^{0.45}$
Kern County[R]	1952/07/21	7.4	1	$180f^{0.45}$
San Fernando[R]	1971/02/09	6.6	10	$180f^{0.45}$
Tabas, Iran[R]	1978/09/16	7.3	1	[5]$87f^{1.46}$
Coalinga-01[R]	1983/05/02	6.3	24	$180f^{0.45}$
Coalinga-02[R]	1983/05/09	5.2	13	$180f^{0.45}$
Coalinga-04[R]	1983/07/09	5.1	9	$180f^{0.45}$
Coalinga-05[R]	1983/07/22	5.7	7	$180f^{0.45}$
Coalinga-07[R]	1983/07/25	5.2	1	$180f^{0.45}$
Nahanni, Canada[R]	1985/12/23	6.7	3	[6]$68f^{1.0}$
Cape Mendocino[R]	1992/04/25	7.2	3	$180f^{0.45}$
Northridge-01[R]	1994/01/17	6.6	63	$180f^{0.45}$
Sierra Madre[R]	1991/06/28	5.6	5	$180f^{0.45}$
Northridge-06[R]	1994/03/20	5.3	20	$180f^{0.45}$

1: Corresponded to [26]; 2: Corresponded to [27]; 3: Corresponded to [28]; 4: Corresponded to [29];

5: Corresponded to [5]; 6: Corresponded to [30].

Table 1. Continued.

Earthquake Name	Date	Magnitude	# of NEHRP C Records	Quality Factor
Chi-Chi, Taiwan-02[R]	1999/09/20	6.3	46	$117f^{0.77}$
Chi-Chi, Taiwan-03[R]	1999/09/20	6.6	45	$117f^{0.77}$
Chi-Chi, Taiwan-05[R]	1999/09/22	6.4	26	$117f^{0.77}$
Chi-Chi, Taiwan-06[R]	1999/09/25	6.5	42	$117f^{0.77}$
Lytle Creek[RO]	1970/09/12	5.3	5	$180f^{0.45}$
Santa Barbara[RO]	1978/08/13	5.8	2	$180f^{0.45}$
Whittier Narrows-01[RO]	1987/10/01	5.9	48	$180f^{0.45}$
Loma Prieta[RO]	1989/10/18	6.9	20	$180f^{0.45}$
Chi-Chi, Taiwan[RO]	1999/09/20	7.6	50	$117f^{0.77}$
Northridge-04[RO]	1994/01/17	5.8	5	$180f^{0.45}$
Northridge-05[RO]	1994/01/17	5.1	6	$180f^{0.45}$
Oroville-04[NO]	1975/08/02	4.4	3	$180f^{0.45}$
Mammoth Lakes-01[NO]	1980/05/25	6.2	1	$180f^{0.45}$
Anza-02[NO]	2001/10/31	5.2	6	$180f^{0.45}$

EXSIM program [3]. In EXSIM, the acceleration spectrum of a subfault at a distance, R_{ij}, is modeled as a point source with a ω^2 shape. The acceleration spectrum of the shear waves of the ijth subfault, $A_{ij}(f)$, is described by Motazedian and Atkinson [3] as:

$$A_{ij}(f) = (CM_{0ij}H_{ij}(2\pi f)^2/[1 + (f/f_{0ij})^2])$$

$$\exp(-\pi f R_{ij}/Q\beta)R_{ij}^b D(f)\exp(-\pi f\kappa), (2)$$

where M_{0ij}, f_{0ij} and R_{ij} are the ijth subfault seismic moment, corner frequency and distance from the observation point, respectively. H_{ij} is a scaling factor that is applied to conserve the square of the high-frequency spectral level of the subfaults as the corner frequency decreases with time [3]. The corner frequency is treated as a dynamic parameter that decreases with time as the rupture grows larger [3]. The corner frequency of the ijth subfault, $f_{0ij}(t)$, is defined as a function of $N_R(t)$, which is the cumulative number of ruptured subfaults at time t:

$$f_{0ij}(t) = \frac{4.9 \times 10^6 \beta}{N_R(T)^{\frac{1}{3}}}\left(\frac{\Delta\sigma}{M_{0ave}}\right)^{\frac{1}{3}}, \quad (3)$$

where $M_{0ave} = M_0/N$ is the average seismic moment of the subfaults in dyne-cm, $\Delta\sigma$ is the stress drop in bars and β is in km/s.

For $t = t_{end}$, the number of ruptured subfaults is $N_R(t)^{-1/3} = N^{-1/3}$. Thus, the corner frequency at the end of the rupture is:

$$f_{0ij}(t_{end}) = N^{-1/3}4.9e + 6\beta(\Delta\sigma/M_0/N)^{1/3},$$

which leads us to $f_{0ij}(t_{end}) = f_0$, which is the corner frequency of the entire fault. Thus, the lower limit of the dynamic corner frequency is the corner frequency of the entire fault. The scaling factor, H_{ij}, which conserves the square of the spectrum amplitude of subfaults at high frequencies, is given by:

$$H_{ij} = \left(N\sum\{f^2/[1 + (f/f_0)^2]\}^2/\right.$$

$$\left.\sum\{f^2/[1 + (f/f_{0ij})^2]\}^2\right)^{\frac{1}{2}}. \quad (4)$$

The ground motions of the subfaults are summed in the time domain to obtain the ground motion acceleration of the entire fault, $a(t)$:

$$a(t) = \sum_{i=1}^{nl}\sum_{j=1}^{nw} a_{ij}(t + \Delta t_{ij}), \quad (5)$$

where Δt_{ij} is the relative delay time for the radiated wave from the ijth subfault to reach the observation point; and, nl and nw are the numbers of subfaults along the length and width of the fault, respectively ($N = nl * nw$).

The EXSIM method, with the application of dynamic corner frequency and the inclusion of the analytical method [31], offers several significant advantages over previous stochastic finite fault models [3]:

- The most frequent criticism of previous stochastic finite fault models, including those by Schneider et al. [11], Silva and Darragh [32] and Beresnev

and Atkinson [20,33,34], has been that the results depend on the selected subfault size. This constraint appears physically unrealistic and places constraints on the subfault sizes that may be used (e.g. the results will only match observations for a limited range of subfault size choices). On the other hand, the EXSIM model is not dependent on subfault size. There is a slight subfault size dependency in the near source, due to the different distribution of distances between the observation point and each subfault. This subfault dependency on a near source is much smaller than the subfault size dependency observed in other approaches, while the subfault size dependency at larger distances is zero.

- In previous approaches, the minimum magnitude that could be simulated as a finite fault was about $M5$ [35]. The methods broke down at smaller magnitudes, because the prescribed subfault size approached the fault size. EXSIM is able to consider much smaller magnitudes. This has major advantages for applications in some regions.

- Another conceptual advantage of the EXSIM model is that it eliminates the need, as in previous approaches [11,20,32], to trigger each subfault a number of times in order to conserve seismic moment.

- Simulations based on the EXSIM approach produce more realistic time series than those based on the previous stochastic finite fault models [20], because in previous approaches, a large subfault size is required to model very large earthquakes (e.g. $M8$), often producing artificial gaps in the simulated acceleration time series. With EXSIM, a small subfault size is chosen to eliminate any such artifacts in the time series.

- Finally, the combination of analytical and stochastic methods proposed by Mavroeidis and Papageorgiou [31] is included in EXSIM, in order to provide a tool to describe the impulsive behavior of near-fault velocity pulses and their influence on long-period ground motions, which are observed in many earthquakes. Thus, it provides a range of tools that cover the stochastic spectrum of finite fault modeling and can be used to investigate the parameters that influence the characteristics of earthquake ground motion.

INPUT PARAMETERS

Stochastic finite fault modeling requires some region specific attenuation and generic site parameters, which are described below:

- Attenuation of Fourier amplitudes with distance. This is the geometric attenuation versus distance, R, for subfaults or point sources. In this research,

to avoid the complexity of geometric spreading (b value) for earthquakes in different regions, only time series with distances less than 60 km with R^{-1} were considered, which was valid for all point sources, as well as all subfaults. The sensitivity of stress drop on this parameter was also investigated.

- Site amplification. Only PEER NGA time series recorded at NHERP C-class sites were modeled in this research, in order to minimize the site effects on the estimation of stress drop. Calibration and simulation were performed for a generic rock site that was equivalent to NEHRP C-class.

- Generic crustal amplification. The California based generic crustal amplification for the rock site proposed by Boore and Joyner [36] was applied for all stations in this research.

- *Kappa* factor. A generic value of 0.035 was considered for all PEER NGA NEHRP C-class site records. The sensitivity of stress drop on this parameter was also investigated.

- Duration of ground motion. The generic $T(R) = T_0 + 0.1R$ from Boatwright and Choy [37] was adopted in this study, where T_0 is the source duration ($T_0 = 1/(2fa)$ and $\log f_a = 2.41 - 0.533M$ after Atkinson and Boore [8]).

- Crustal shear wave velocity. A generic value of 3.7 (km/s) was chosen for this parameter, which does not have a significant influence on the stress drop.

- Crustal density. A generic value of 2.8 (g/cm^3) was chosen for this parameter, which does not have a significant influence on the stress drop.

- Slip distribution. A random slip distribution was assumed, since the focus was a general calibration of the model parameters.

- Fault geometry. The fault geometry of each fault was obtained from the PEER NGA database and literature.

- Location of hypocenter. This location was determined on the fault plane, based on the fault geometry and the reported coordinate for the hypocenter.

- Pulsing percentage. This parameter which controls the level of spectrum at low frequencies was fixed on 100% for all simulations, but it did not play an important role in this research, since the focus was on stress drop; a high-frequency parameter.

- Rupture velocity. It was assumed that the rupture velocity is 80% of the shear wave velocity, and the Saragoni-Hart function was used as the windowing function in our simulation.

- Subfault size. In near source where there is a slight subfault size, dl, dependency, the Beresnev and Atkinson (1999) equation ($\log dl = -2.0 + 0.4M$)

was used for the calculation of the size of sub-faults [35].

- Q value. This parameter is inversely related to the anelastic attenuation of seismic waves and determines the shape of the high-frequency spectrum. Although Q values, listed in Table 1, were obtained from literature for each region, this parameter does not play a significant role at distances less than 60 km, which is the maximum distance limit in this research.

- Stress drop. This parameter controls the level of spectrum at high frequencies. The main goal of this research was to determine the average of this parameter using trial and error, as described in the next section.

CALIBRATION RESULTS

Using the above-mentioned input parameters, EXSIM was applied to simulate the acceleration time series for each NEHRP C record located at a distance less than 60 km. The geometry of each fault and the location of each site were considered in each simulation. The PSA of the simulated time series is compared with the PSA given by the PEER NGA database. The stress drop is estimated by trial and error, based on matching the observed PSA with the simulation results. A suitable value for stress drop produces a good distribution of residuals at high frequencies where the residual is defined as the log of the observed PSA minus the log of the predicted PSA (where PSA is the horizontal component of 5% damped pseudo acceleration). The symmetric distribution of residuals around the zero line without any specific trend at high frequencies can be considered an indicator of good agreement between the simulated and observed time series. It should be added that there are some minor to moderate trends at lower frequencies that do not have any effect on our conclusions and the estimation of stress drop. These low-frequency trends can be corrected using the analytical modeling in EXSIM, which is not within the scope of this research.

The level of high frequencies, mainly above 1 Hz, is controlled by three factors: the stress drop, $Kappa$ factor and Q value. The variation of the $Kappa$ factor is not significant for NHERP C-class sites and is considered to be 0.035 in this research. Some sensitivity analysis was also done on this parameter. The Q value is a known parameter (from the literature) and does not play a significant role at short distances (less than 60 km, which is the maximum distance considered in this research). Thus, the stress drop is the main parameter controlling the level of spectrum at high frequencies for the chosen subset of the PEER NGA database, and can be estimated with iteration over a wide range of values.

The EXSIM program, using the above-mentioned input parameters, was applied over a wide range of stress drops to minimize the residuals for each earthquake in the selected database. Table 2 includes the estimated stress drops based on stochastic finite fault modeling, as well as the current PEERNGA static stress drops.

In addition, stress drop values were also calculated for all earthquakes based on point source modeling. The EXSIM program can be used for point source modeling, and its results are identical to the SMSIM program [7]. Motions from EXSIM are in close agreement with those from SMSIM, far from small earthquakes [38]. The input parameters for point source modeling were the same as those for finite fault modeling, except that the number of subfaults was 1 and the hypocenter was located at the middle of the only subfault.

Static stress drops which have been presented by the NGA database are used in this article. Static stress drop is the difference between the stresses before and after an earthquake. Small static stress drop shows that the strain energy is not released in the crust and probably the region will experience some aftershocks. Brune stress drop can be used in stochastic point source simulation applying the SMSIM developed by David Boore [7]. Another kind of stress drop is the finite fault stress drop, which was regarded in this research as well. Table 2 also includes the estimated stress drops based on point source modeling.

Stress drop does not actually have the same meaning in EXSIM and SMSIM. In SMSIM, it comes directly from the Brune source model for a given stress parameter in which the stress drop, corner frequency and seismic moment control the spectral amplitudes, however, in EXSIM, it has this meaning only for a particular subsource [39].

In order to separate results of different qualities, a simulation quality parameter was defined, based on the visual inspection of the goodness of the average distribution of residual versus frequency. This parameter has 3 grades: A, B and C. If residuals were very close to the zero line over the frequency range of 1 Hz to 10 Hz, this parameter was considered grade A, which shows the simulation results were very good (as an example, see residuals for the Livermore earthquake in Figure 1). In cases where the residuals were not close to the zero line for a short range of frequencies, the simulation quality was B (see Table 2 and Figure 1). Simulation quality C was chosen for the worst case where residuals deviated from the zero line in a relatively wide range of frequencies.

In order to compare the estimated stress drop values of different methods, the stress drop based on stochastic finite fault modeling was considered as a reference, and the percentage difference between the

Table 2. Estimated stress drops based on stochastic modeling for the PEER NGA database.

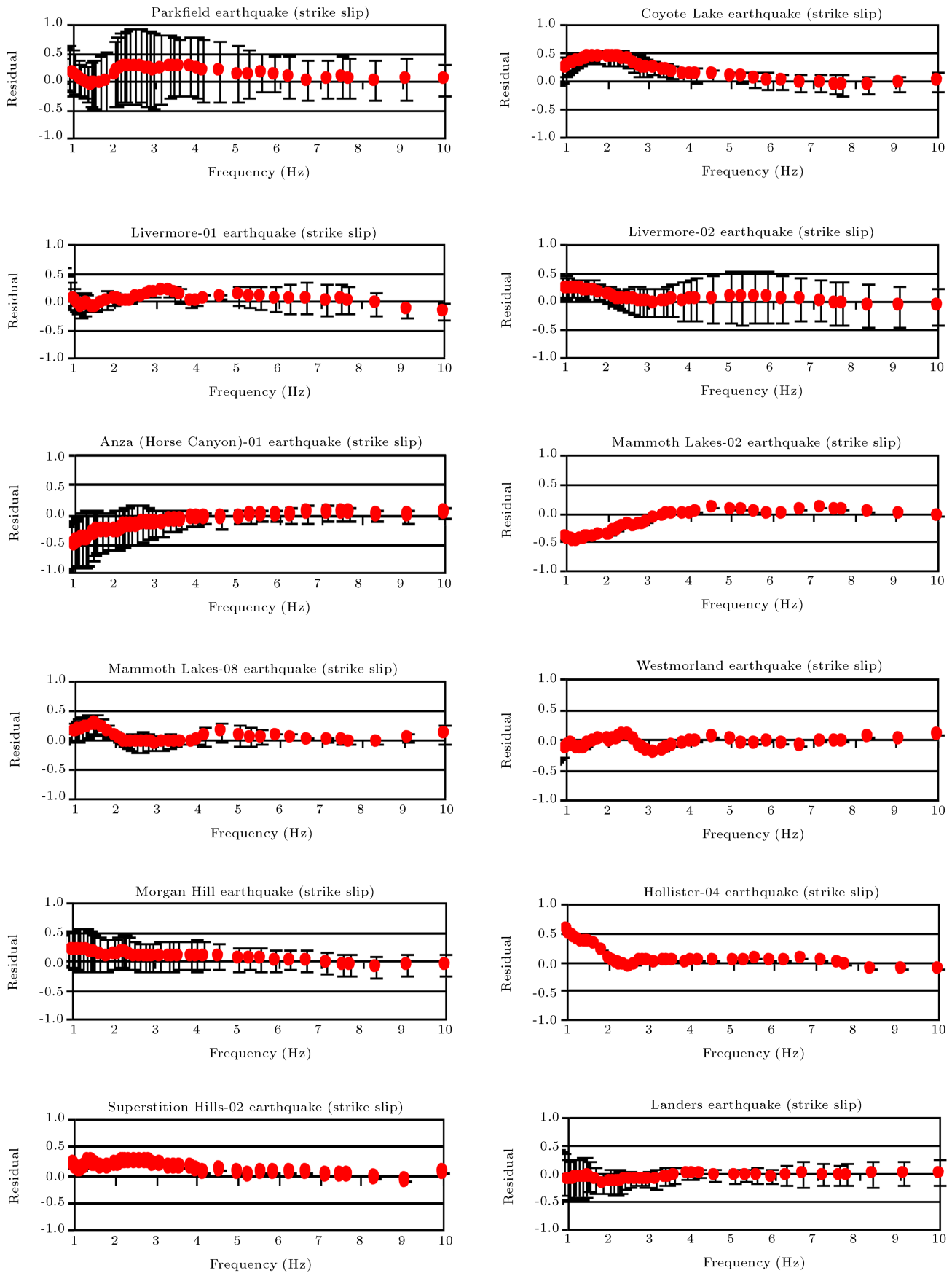| Earthquake Name	Magnitude	PEER-NGA Static Stress Drop (bars)	Stress Drop Based on Point Source Modeling (bars)	Stress Drop Based on Finite Fault Modeling (bars)	No. of Records	Simulation Quality
Parkfield	6.2	10.2	120	50	2	B
Coyote Lake	5.7	35.5	75	50	5	B
Livermore-01	5.8	-	120	80	2	A
Livermore-02	5.8	-	135	100	3	A
Anza (Horse Canyon)-01	5.6	-	125	100	3	B
Mammoth Lakes-02	6.0	20.2	290	200	1	C
Mammoth Lakes-08	4.9	-	210	140	2	B
Westmorland	5.9	33.0	120	100	1	A
Morgan Hill	6.1	9.6	130	70	9	A
Hollister-04	5.4	-	45	40	1	B
Superstition Hills-02	6.5	47.5	95	85	1	A
Landers	7.3	64.5	75	40	4	A
Big Bear-01	6.5	-	115	100	2	A
Hector Mine	7.1	36.2	125	80	2	A
Yountville	5.2	-	45	40	3	B
Big Bear-02	5.3	-	55	40	9	C
Gilroy	5.2	-	100	65	7	A
Chi-Chi, Taiwan-04	6.4	7.5	60	30	1	B
Oroville-02	4.8	-	30	25	2	B
Oroville-03	4.7	-	100	80	8	C
Irpinia, Italy-01	6.9	32.7	210	150	3	A
Irpinia, Italy-02	6.2	29.2	120	90	2	A
Lazio-Abruzzo, Italy	5.9	40.4	120	100	1	B
Kozani, Greece-01	6.5	12.5	110	100	1	B
Little Skull Mtn, NV	5.7	37.8	180	110	1	C
Kern County	7.4	82.3	100	90	1	A
San Fernando	6.6	24.5	185	160	10	A
Tabas, Iran	7.3	16.4	400	250	1	A
Coalinga-01	6.3	40.6	115	90	24	C
Coalinga-02	5.2	-	210	150	13	A
Coalinga-04	5.1	-	245	170	9	A
Coalinga-05	5.7	-	200	155	7	A
Coalinga-07	5.2	-	270	230	1	A
Nahanni, Canada	6.7	26.2	45	40	3	A
Cape Mendocino	7.2	67.6	150	120	3	A
Northridge-01	6.6	33.0	200	165	63	A
Sierra Madre	5.6	103.2	400	290	5	B
Northridge-06	5.3	-	205	130	20	A
Chi-Chi, Taiwan-02	6.3	5.0	55	40	46	A
Chi-Chi, Taiwan-03	6.6	47.3	30	20	45	C
Chi-Chi, Taiwan-05	6.4	9.0	180	155	26	A
Chi-Chi, Taiwan-06	6.5	5.5	70	50	42	C
Lytle Creek	5.3	-	250	160	5	A
Santa Barbara	5.8	58.6	80	60	2	C
Whittier Narrows-01	5.9	56.8	285	235	48	A
Loma Prieta	6.9	35.1	140	100	20	A
Chi-Chi, Taiwan	7.6	34.9	55	30	50	C
Northridge-04	5.8	-	110	75	5	B
Northridge-05	5.1	-	160	90	6	B
Oroville-04	4.4	-	115	100	3	B
Mammoth Lakes-01	6.2	18.3	70	50	1	B
Anza-02	5.2	-	260	180	6	C

Figure 1. Average of residuals versus frequency for all analyzed earthquakes (continued).
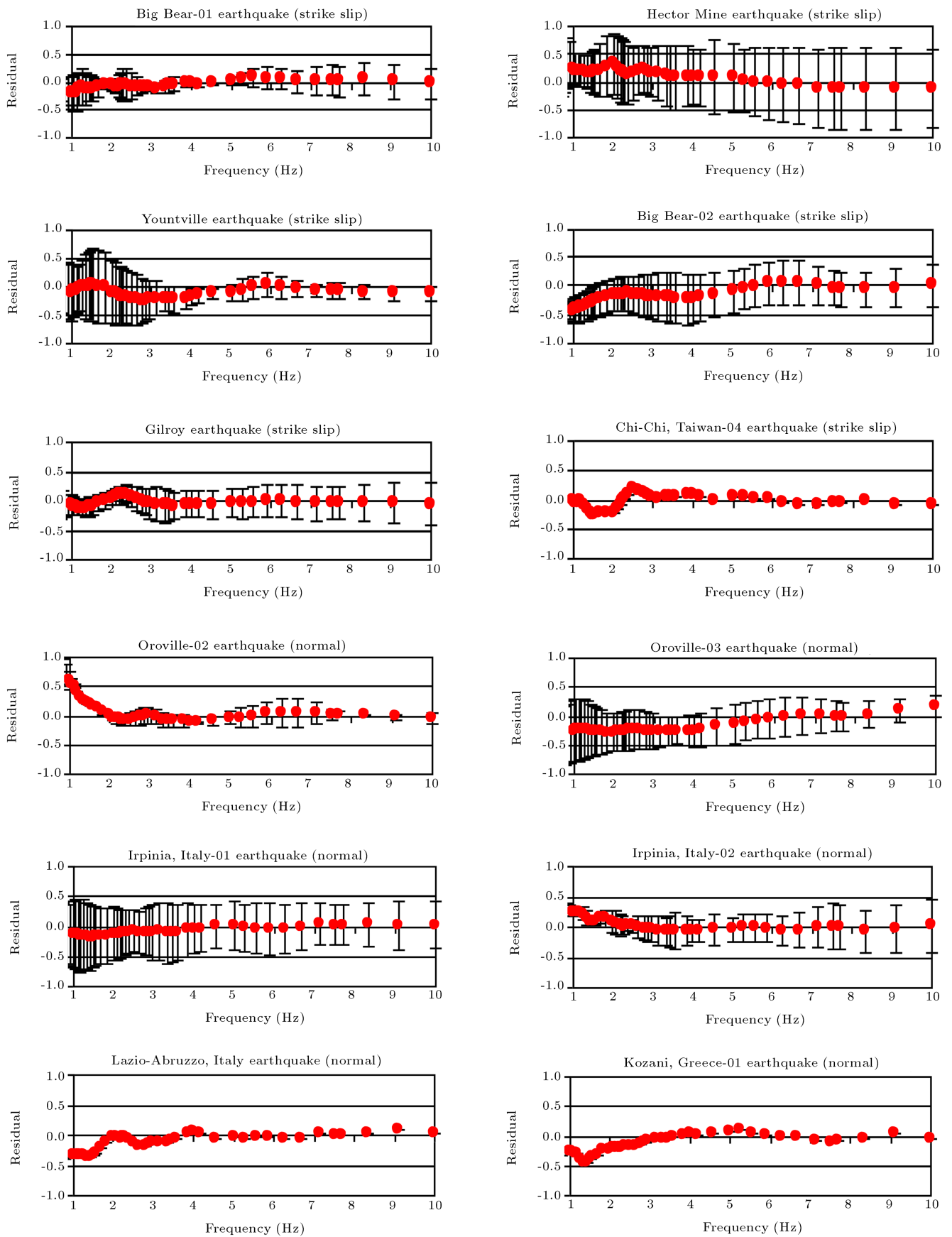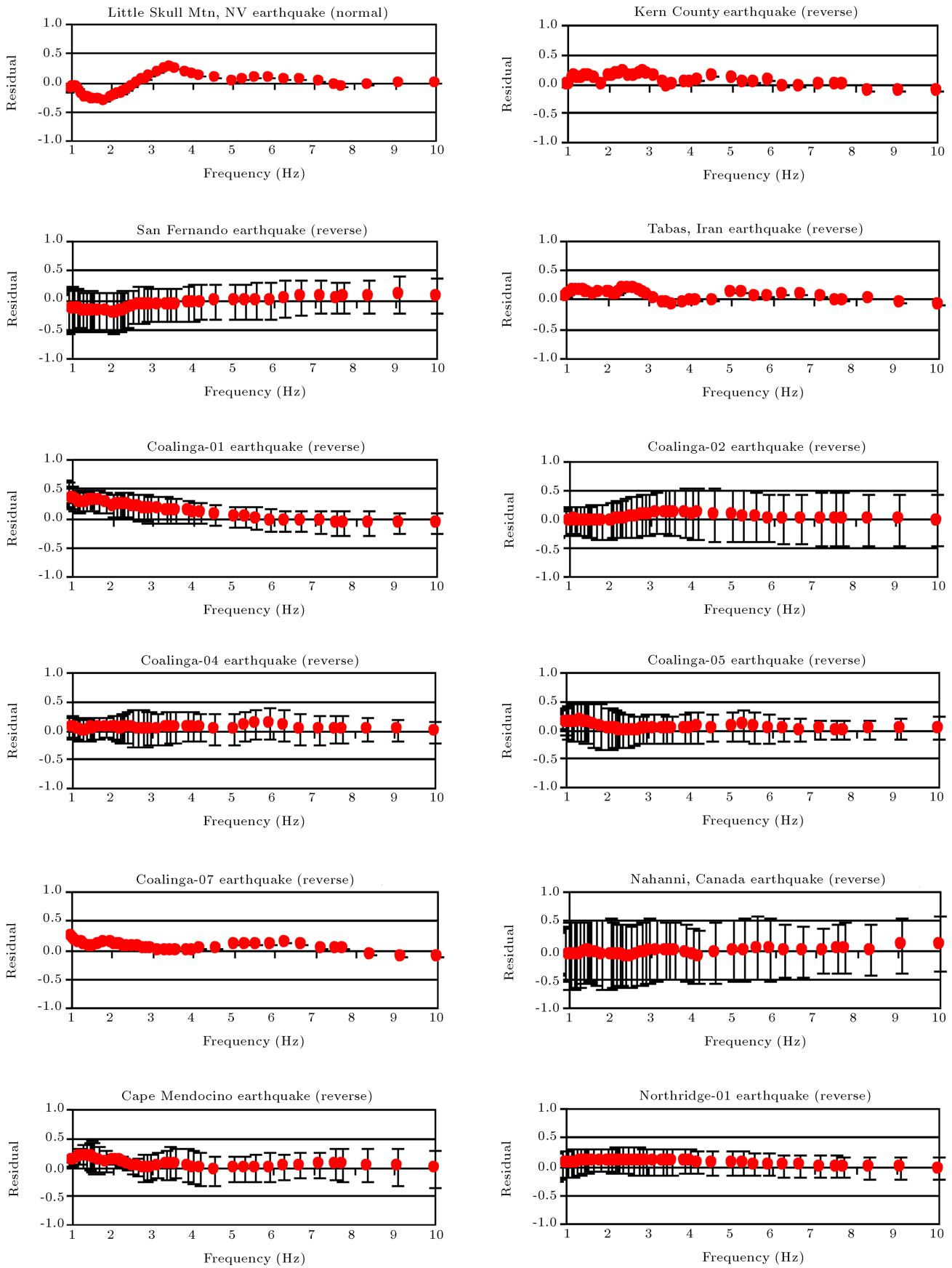
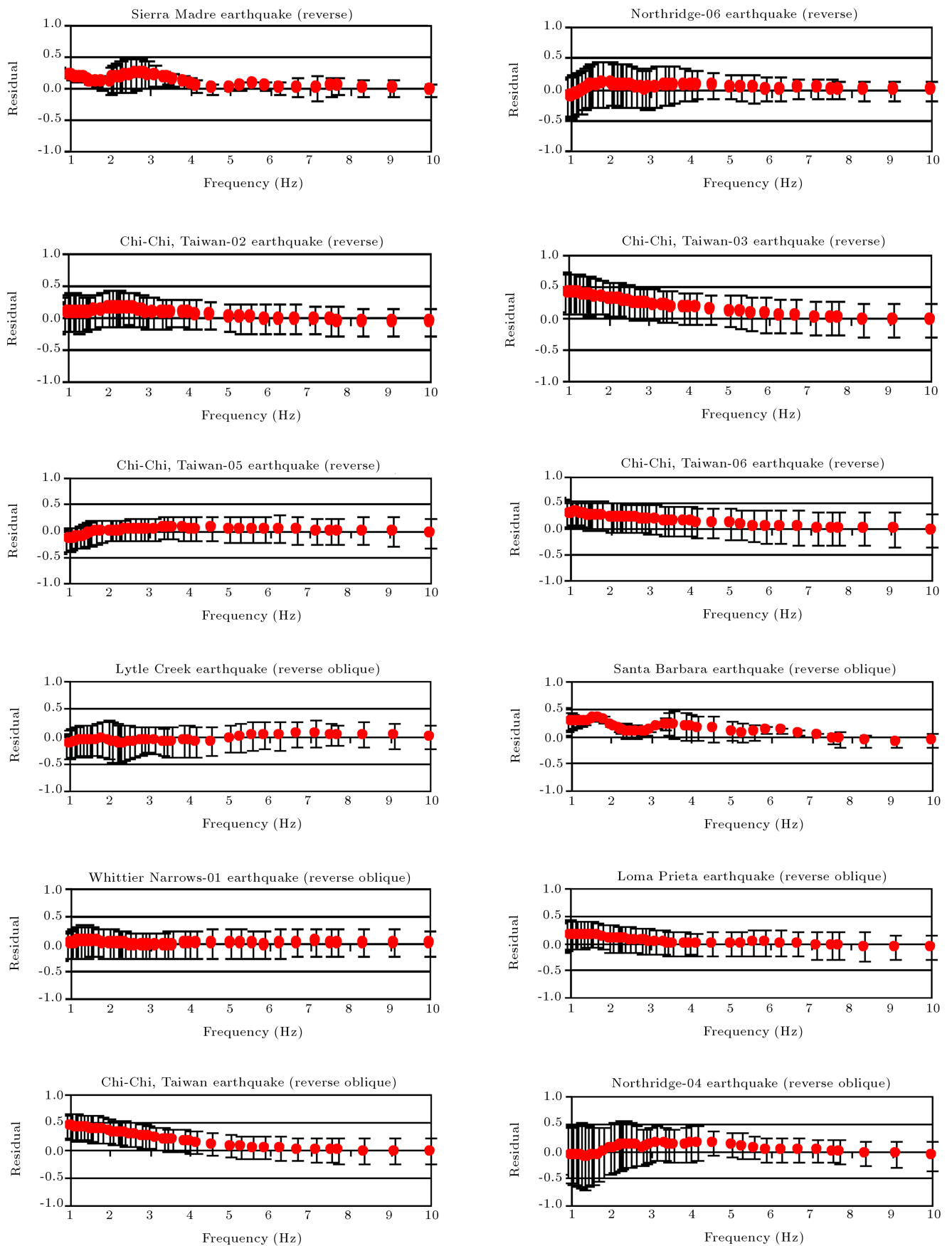**Figure 1.** Continued.

Figure 1. Continued.
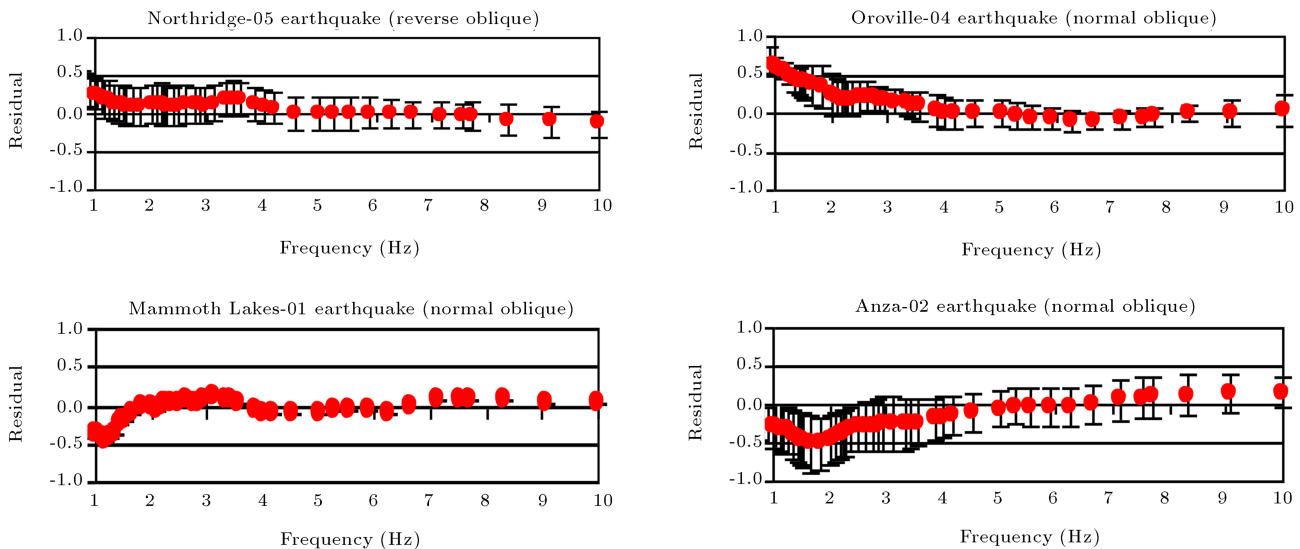
Figure 1. Continued.

Figure 1. Continued.

stress drop values from other methods and the reference method was calculated. Two distributions were plotted versus the reference stress drop, as shown in Figure 2. The first distribution (solid circle) shows (Point Source Stress Drop - Finite Fault Stress Drop)/(Finite Fault Stress Drop)*100; and the second distribution shows (PEER-NGA Static Stress Drop - Finite Fault Stress Drop)/(Finite Fault Stress Drop)*100. As shown in Figure 2, for all earthquakes, stress drops based on stochastic point source modeling were generally greater than the corresponding values based on stochastic finite fault modeling. This subject is discussed below.

In case of considering the whole fault as a sub-fault, the fault is modeled as a point source. If the finite fault modeling is used and the fault is divided into several subfaults, then the seismic moments of subfaults will reduce and their corresponding corner frequencies will increase. Consequently, the content of high frequencies is greater in finite fault modeling, in comparison with that of point source modeling. As such high frequencies are not attenuated at near distances, it is concluded that finite fault modeling produces larger spectral accelerations in comparison to point modeling, assuming the same stress drop values in both cases. Therefore, if the modeled accelerations at high frequencies are to be fitted to the spectral accelerations of real records by changing the stress drop, then the stress drop obtained by finite fault modeling is lower in comparison with that of point source modeling.

For most earthquakes, the PEER-NGA static stress drops were typically smaller than the calculated stress drops based on finite fault modeling and point source modeling.

Calculated stress drops based on stochastic point source and finite fault modeling versus magnitude are

also shown in Figure 3. It is clear that there was no relation between the stochastic stress drops and the magnitude of the earthquakes.

For all the studied earthquakes, Table 2 shows the lowest stress drop values for the Chi-Chi, Taiwan-03 earthquake. For this earthquake, the calculated stress drops were 30 and 20 bars, based on stochastic point source and finite fault modeling, respectively. The highest stress drop values were obtained for the Sierra Madre earthquake, which were 400 and 290 bars, based on stochastic point source and finite fault modeling, respectively. The PEER NGA database presents a high stress drop (103.2 bars) for that earthquake as well.

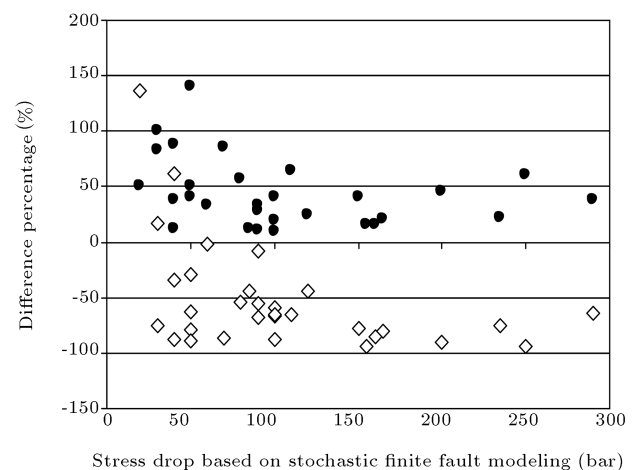**Figure 2.** Comparison between static PEER NGA and stochastic stress drops. Solid circles shows (Point Source Stress Drop - Finite Fault Stress Drop)/(Finite Fault Stress Drop)*100. Diamonds show (PEER NGA Static Stress Drop - Finite Fault Stress Drop)/(Finite Fault Stress Drop)*100.
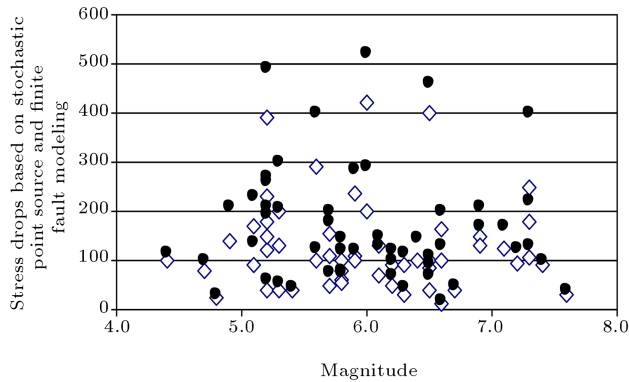
Figure 3. Calculated stress drops based on stochastic point source (solid circles) and finite fault modeling (diamonds) versus magnitude.

In order to evaluate the utilized generic geometric spreading factors, the distribution of residuals (obtained from stochastic finite fault modeling) versus distance for two earthquakes (Northridge-01 and Whittier Narrows-01), as examples, were plotted for the frequency of 5 Hz, and are shown in Figures 4 and 5, which indicate no obvious trends.

DEPENDENCY OF STRESS DROP ON *KAPPA* FACTOR AND *B* VALUE

Both the *Kappa* factor and *b* value were changed by ±10% (based on comments made by Gail Atkinson) in both stochastic point source and finite fault sim-
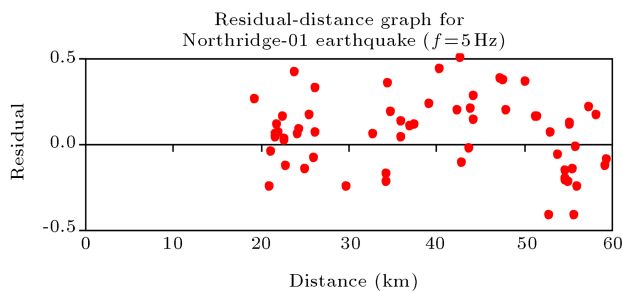

Figure 4. Distribution of residuals versus distance for 5 Hz frequency for the Northridge-01 earthquake.
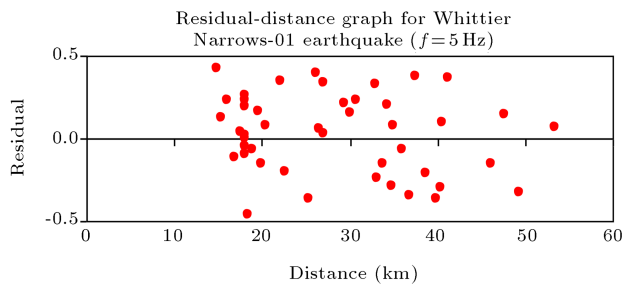

Figure 5. Distribution of residuals versus distance for 5 Hz frequency for the Whittier Narrows-01 earthquake.

ulations, which resulted in 9 scenarios for each type of stochastic simulation (three values for the *Kappa* factor and three values for the *b* value). First, as a base, the simulation was done for the typical and generic values of these parameters (*Kappa* = 0.035 and *b* = 1.0). These parameters were then changed individually, and their effects on the estimated stress drop were calculated, as given in Tables 3 and 4 for stochastic point source modeling and stochastic finite fault modeling, respectively.

It is clear that, if the *Kappa* factor was increased, the simulated spectral accelerations at high frequencies, typically more than 5 Hz, decreased, and vice versa. On the other hand, the estimation of stress drop was directly related to the level of spectrum at high frequencies. In other words, in order to match the simulated spectrum with the observed one, an increase in the *Kappa* factor meant that the associated stress drop had to be increased. It is interesting that an increase in the typical value of the *Kappa* factor resulted in an increase in the stress drop by the same value, i.e. a 10% increase in the *Kappa* factor would result in a 10% increase in the estimated stress drops, regardless of the hypocentral distance. This phenomenon was observed in all simulations using both stochastic point source and finite fault simulations.

Theoretically speaking, the simulated spectrum is inversely related to the *b* value (because the geometric speeding factor follows the form of $1/R^b$). This means that any increase in the *b* value results in lower amplitudes for the simulated spectrum; therefore, the stress drop should be increased to match the simulated spectrum with the recorded one. Our simulations for all earthquakes suggest that any change in the *b* value results in a higher and distance dependent change in the estimated stress drop. It should be mentioned that any change in the *b* value changes the weight of R (distance) in the simulation; thus, the effect of the *b* value is tied to the value of R. In other words, any change in the *b* value changes the simulated spectrum through the R parameter, and changes in the estimated stress drop are distance dependent. Our simulations suggest that, depending on the distance, a 10% increase in the typical *b* value results in a 30-80% increase in the stress drop, while a 10% decrease in the *b* value causes a 20-50% decrease in the stress drop. Based on the values given in Tables 3 and 4, as well as theoretical judgment, one can conclude that the effect of changes in the *b* value on the stress drops is higher for a larger R.

If both the *Kappa* factor and *b* value are changed simultaneously, the new stress drops can be estimated by adding the separate effects of both factors. For example, if the estimated stress drop for typical values of the *Kappa* factor and *b* value (0.035 and 1.0, respectively) is $\Delta\sigma_.$, the effect of any changes in the

Table 3. Estimated stress drops based on stochastic point source modeling for the PEER NGA database for different *Kappa* factors and *b* values (continued).

Earthquake Name	K=0.035, b = 1.0	K=0.9* 0.035, b = 1.0	K=1.1* 0.035, b = 1.0	K=0.035, b = 0.9	K=0.035, b = 1.1	K=0.9* 0.035, b = 0.9	K=1.1* 0.035, b = 0.9	K=0.9* 0.035, b = 1.1	K=1.1* 0.035, b = 1.1
Parkfield	120	108	132	72	185	60	84	173	197
Coyote Lake	75	68	83	45	105	38	53	98	113
Livermore-01	120	108	132	70	190	58	82	178	202
Livermore-02	135	122	149	80	210	67	94	197	224
Anza (Horse Canyon)-01	125	113	138	75	190	63	88	178	203
Mammoth Lakes-02	290	261	319	175	425	146	204	396	454
Mammoth Lakes-08	210	189	231	125	295	104	146	274	316
Westmorland	120	108	132	70	170	58	82	158	182
Morgan Hill	130	117	143	80	200	67	93	187	213
Hollister-04	45	41	50	30	75	26	35	71	80
Superstition Hills-02	95	86	105	60	130	51	70	121	140
Landers	75	68	83	45	120	38	53	113	128
Big Bear-01	115	104	127	70	185	59	82	174	197
Hector Mine	125	113	138	75	190	63	88	178	203
Yountville	45	41	50	26	80	22	31	76	85
Big Bear-02	55	50	61	35	85	30	41	80	91
Gilroy	100	90	110	60	150	50	70	140	160
Chi-Chi, Taiwan-04	60	54	66	35	95	29	41	89	101
Oroville-02	30	27	33	23	50	20	26	47	53
Oroville-03	100	90	110	70	140	60	80	130	150
Irpinia, Italy-01	210	189	231	140	330	119	161	309	351
Irpinia, Italy-02	120	108	132	80	170	68	92	158	182
Lazio-Abruzzo, Italy	120	108	132	80	185	68	92	173	197
Kozani, Greece-01	110	99	121	70	160	59	81	149	171
Little Skull Mtn, NV	180	162	198	135	265	117	153	247	283
Kern County	100	90	110	60	160	50	70	150	170
San Fernando	185	167	204	105	300	87	124	282	319
Tabas, Iran	400	360	440	240	640	200	280	600	680
Coalinga-01	115	104	127	65	190	54	77	179	202
Coalinga-02	210	189	231	140	315	119	161	294	336
Coalinga-04	245	221	270	160	365	136	185	341	390
Coalinga-05	200	180	220	135	290	115	155	270	310
Coalinga-07	270	243	297	180	400	153	207	373	427
Nahanni, Canada	45	41	50	30	65	26	35	61	70
Cape Mendocino	150	135	165	95	230	80	110	215	245
Northridge-01	200	180	220	130	330	110	150	310	350
Sierra Madre	400	360	440	250	600	210	290	560	640
Northridge-06	205	185	226	135	330	115	156	310	351
Chi-Chi, Taiwan-02	55	50	61	30	100	25	36	95	106
Chi-Chi, Taiwan-03	30	27	33	20	50	17	23	47	53
Chi-Chi, Taiwan-05	180	162	198	105	290	87	123	272	308

Table 3. Continued.

Earthquake Name	$K=0.035$, $b=1.0$	$K=0.9*$ 0.035, $b=1.0$	$K=1.1*$ 0.035, $b=1.0$	$K=0.035$, $b=0.9$	$K=0.035$, $b=1.1$	$K=0.9*$ 0.035, $b=0.9$	$K=1.1*$ 0.035, $b=0.9$	$K=0.9*$ 0.035, $b=1.1$	$K=1.1*$ 0.035, $b=1.1$
Chi-Chi, Taiwan-06	70	63	77	40	120	33	47	113	127
Lytle Creek	250	225	275	160	390	135	185	365	415
Santa Barbara	80	72	88	50	140	42	58	132	148
Whittier Narrows-01	285	257	314	180	430	152	209	402	459
Loma Prieta	140	126	154	85	220	71	99	206	234
Chi-Chi, Taiwan	55	50	61	30	90	25	36	85	96
Northridge-04	110	99	121	65	185	54	76	174	196
Northridge-05	160	144	176	100	255	84	116	239	271
Oroville-04	115	104	127	80	180	69	92	169	192
Mammoth Lakes-01	70	63	77	50	115	43	57	108	122
Anza-02	260	234	286	155	390	129	181	364	416

Kappa factor in the stress drop is $\Delta\sigma_\kappa$ and the effect of any changes in the b value (for a specific range of distances) is $\Delta\sigma_b$; thus, the resulting stress drop is $\Delta\sigma. + \Delta\sigma_\kappa + \Delta\sigma_b$ (This point can be proven mathematically). Based on the values given in Tables 3 and 4 (which were expected theoretically as well), the maximum values of stress drop for earthquakes were for a higher *Kappa* factor (1.1*0.035) and a higher b value (1.1), and the minimum estimated stress drops were for a lower *Kappa* factor (0.9*0.035) and a lower b value (0.9).

CONCLUSION

In this study, 541 records from the PEER NGA database of 52 large shallow earthquakes from all over the world, with magnitudes ranging from $M4.4$ to $M7.6$, were simulated, and their acceleration response spectra were analyzed to obtain the stress drops based on stochastic point source and finite fault modeling. In order to minimize the site effect, the PSA of accelerograms recorded on just the rock sites (NEHRP C-class) was considered. The simulations were based on both stochastic point source and finite fault modeling, and the stress drops were calculated for each earthquake separately based on their fault locations and geometries. The calculation of stress drops was done based on the analysis of residuals versus magnitude, distance and frequency. Residuals were calculated for each record at each frequency where the residual is defined as the log of the observed PSA minus the log of the predicted PSA.

For all earthquakes, the calculated stress drops based on stochastic finite fault modeling were smaller than the corresponding values based on stochastic point source modeling. Both of these stress drop values were different from the static stress drop values that are listed in the current PEER NGA database. For most of the earthquakes, the static stress drops were smaller than the calculated stress drops in this research. It seems that there was no relation between estimated stress drop and the magnitude of the earthquake, but there is a good linear relation between the estimated stress drops based on stochastic point source and finite fault modeling.

As expected theoretically, any increase in the *Kappa* factor, as an input parameter in the stochastic modeling, increased the estimated stress drop by the same factor. The effect of the b value, another important input parameter, on the estimated stress drop was distance dependent, and any increase in the b value caused an increase in the estimated stress drop; more severe for far-field records.

DATA SOURCES

All observed data were obtained from the response spectra database compiled by Pacific Engineering & Analysis.

Table 4. Estimated stress drops based on stochastic finite fault modeling for the PEER NGA database for different *Kappa* factors and *b* values (continued).

Earthquake Name	K=0.035, b = 1.0	K=0.9* 0.035, b = 1.0	K=1.1* 0.035, b = 1.0	K=0.035, b = 0.9	K=0.035, b = 1.1	K=0.9* 0.035, b = 0.9	K=1.1* 0.035, b = 0.9	K=0.9* 0.035, b = 1.1	K=1.1* 0.035, b = 1.1
Parkfield	50	45	55	38	85	33	43	80	90
Coyote Lake	50	45	55	38	66	33	43	61	71
Livermore-01	80	72	88	60	125	52	68	117	133
Livermore-02	100	90	110	75	160	65	85	150	170
Anza (Horse Canyon)-01	100	90	110	60	160	50	70	150	170
Mammoth Lakes-02	200	180	220	150	290	130	170	270	310
Mammoth Lakes-08	140	126	154	105	200	91	119	186	214
Westmorland	100	90	110	60	160	50	70	150	170
Morgan Hill	70	63	77	45	110	38	52	103	117
Hollister-04	40	36	44	30	65	26	34	61	69
Superstition Hills-02	85	77	94	64	120	56	73	112	129
Landers	40	36	44	20	60	16	24	56	64
Big Bear-01	100	90	110	65	170	55	75	160	180
Hector Mine	80	72	88	50	125	42	58	117	133
Yountville	40	36	44	20	60	16	24	56	64
Big Bear-02	40	36	44	20	70	16	24	66	74
Gilroy	65	59	72	40	105	34	47	99	112
Chi-Chi, Taiwan-04	30	27	33	17	50	14	20	47	53
Oroville-02	25	23	28	18	40	16	21	38	43
Oroville-03	80	72	88	55	125	47	63	117	133
Irpinia, Italy-01	150	135	165	100	225	85	115	210	240
Irpinia, Italy-02	90	81	99	60	125	51	69	116	134
Lazio-Abruzzo, Italy	100	90	110	65	140	55	75	130	150
Kozani, Greece-01	100	90	110	65	155	55	75	145	165
Little Skull Mtn, NV	110	99	121	70	170	59	81	159	181
Kern County	90	81	99	65	135	56	74	126	144
San Fernando	160	144	176	112	230	96	128	214	246
Tabas, Iran	250	225	275	175	360	150	200	335	385
Coalinga-01	90	81	99	65	140	56	74	131	149
Coalinga-02	150	135	165	105	220	90	120	205	235
Coalinga-04	170	153	187	120	265	103	137	248	282
Coalinga-05	155	140	171	110	240	95	126	225	256
Coalinga-07	230	207	253	160	325	137	183	302	348
Nahanni, Canada	40	36	44	30	55	26	34	51	59
Cape Mendocino	120	108	132	85	175	73	97	163	187
Northridge-01	165	149	182	115	250	99	132	234	267
Sierra Madre	290	261	319	205	420	176	234	391	449
Northridge-06	130	117	143	90	190	77	103	177	203
Chi-Chi, Taiwan-02	40	36	44	30	70	26	34	66	74
Chi-Chi, Taiwan-03	20	18	22	15	35	13	17	33	37
Chi-Chi, Taiwan-05	155	140	171	110	245	95	126	230	261

Table 4. Continued.

Earthquake Name	K=0.035, $b = 1.0$	K=0.9* 0.035, $b = 1.0$	K=1.1* 0.035, $b = 1.0$	K=0.035, $b = 0.9$	K=0.035, $b = 1.1$	K=0.9* 0.035, $b = 0.9$	K=1.1* 0.035, $b = 0.9$	K=0.9* 0.035, $b = 1.1$	K=1.1* 0.035, $b = 1.1$
Chi-Chi, Taiwan-06	50	45	55	35	85	30	40	80	90
Lytle Creek	160	144	176	100	245	84	116	229	261
Santa Barbara	60	54	66	40	100	34	46	94	106
Whittier Narrows-01	235	212	259	150	360	127	174	337	384
Loma Prieta	100	90	110	60	155	50	70	145	165
Chi-Chi, Taiwan	30	27	33	20	50	17	23	47	53
Northridge-04	75	68	83	40	130	33	48	123	138
Northridge-05	90	81	99	50	140	41	59	131	149
Oroville-04	100	90	110	65	170	55	75	160	180
Mammoth Lakes-01	50	45	55	40	75	35	45	70	80
Anza-02	180	162	198	105	270	87	123	252	288

REFERENCES

1. Atkinson, G.M. "Empirical attenuation of ground-motion spectral amplitudes in Southeastern Canada and the Northeastern United States", *Bull. Seism. Soc. Am.*, **94**, pp. 1079-1095 (2004).

2. Motazedian, D. and Atkinson, G.M. "Ground motion relations for Puerto Rico", *Geological Soc. Am., Special Issue on Neotectonics of Puerto Rico, Special Paper*, **385**, pp. 61-80 (2005).

3. Motazedian, D. and Atkinson, G.M. "Stochastic finite fault modeling based on a dynamic corner frequency", *Bull. Seism. Soc. Am.*, **95**, pp. 995-1010 (2005).

4. Motazedian, D. "Region-specific key seismic parameters for earthquakes in Northern Iran", *Bull. Seism. Soc. Am.*, **96**, pp. 1383-1395 (2006).

5. Motazedian, D. and Moinfar, A.A. "Hybrid stochastic finite fault modeling of 2003, M6.5, Bam Earthquake (Iran)", *J. Seism.*, pp. 1-21 (2006).

6. Boore, D.M. "Stochastic simulation of high-frequency ground motions based on seismological models of the radiated spectra", *Bull. Seism. Soc. Am.*, **73**, pp. 1865-1894 (1983).

7. Boore, D.M. "SMSIM-fortran programs for simulating ground motions from earthquakes", *US Geol. Surv., Open-file Report 96-80-A* (1996).

8. Atkinson, G.M. and Boore, D.M. "New ground motion relations for Eastern North America", *Bull. Seism. Soc. Am.*, **85**, pp. 17-30 (1995).

9. Atkinson, G.M. and Silva, W. "Stochastic modeling of California ground motions", *Bull. Seism. Soc. Am.*, **90**, pp. 255-274 (2000).

10. Somerville, P., Sen, M. and Cohee, B. "Simulations of strong ground motions recorded during the 1985 Michoacan, Mexico and Valparaiso, Chile, earthquakes", *Bull. Seism. Soc. Am.*, **81**, pp. 1-27 (1991).

11. Schneider, J., Silva, W. and Stark, C. "Ground motion model for the 1989 M 6.9 Loma Prieta earthquake including effects of source, path and site", *Earthquake Spectra*, **9**, pp. 251-287 (1993).

12. Tumarkin, A. and Archuleta, R. "Empirical ground motion prediction", *Annali Di Geofisica*, **37**, pp. 1691-1720 (1994).

13. Zeng, Y., Anderson, J. and Yu, G. "A composite source model for computing realistic synthetic strong ground motions", *Geophysical Research Letters*, **21**, pp. 725-728 (1994).

14. Beresnev, I. and Atkinson, G.M. "Stochastic finite-fault modeling of ground motions from the 1994 Northridge, California earthquake. I. Validation on rock sites", *Bull. Seism. Soc. Am.*, **88**, pp. 1392-1401 (1998).

15. Atkinson, G.M. and Silva, W. "Empirical source spectra for California earthquakes", *Bull. Seism. Soc. Am.*, **87**, pp. 97-113 (1997).

16. Hartzell, S. "Earthquake aftershocks as Green's functions", *Geophys. Res. Letters*, **5**, pp. 1-14 (1978).

17. Irikura, K. "Semi-empirical estimation of strong ground motions during large earthquakes", *Bull. Disaster Prevention Res. Inst.*, Kyoto University, **33**, pp. 63-104 (1983).

18. Joyner, W.B. and Boore, D.M. "On simulating large earthquakes by Green's function addition of smaller earthquakes in earthquake source mechanics", *American Geophysical Union Monograph*, **37**, pp. 269-274 (1986).

19. Heaton, T. and Hartzell, S. "Source characteristics of hypothetical subduction earthquakes in the Northwestern United States", *Bull. Seism. Soc. Am.*, **76**, pp. 675-708 (1986).

20. Beresnev, I. and Atkinson, G.M. "FINSIM - a FOR-TRAN program for simulating stochastic acceleration time histories from finite faults", *Seism. Res. L.*, **69**, pp. 27-32 (1998).

21. Moghaddam, H., Fanaie, N. and Hamzehloo, H. "Uniform hazard response spectra and ground motions for Tabriz", *Journal of Scientia Iranica, Trans. A*, **16**(3), pp. 238-248 (2009).

22. Boore, D.M. "Simulation of ground motion using the stochastic method", *Pure Appl. Geophys.*, **160**, pp. 636-676 (2003).

23. Aki, K. "Scaling law of seismic spectrum", *J. Geophys. Res.*, **72**, pp. 1217-1231 (1967).

24. Brune, J. "Tectonic stress and the spectra of seismic shear waves from earthquakes", *J. Geophys. Res.*, **75**, pp. 4997-5009 (1970).

25. Anderson, J. and Hough, S. "A model for the shape of the Fourier amplitude spectrum of acceleration at high frequencies", *Bull. Seism. Soc. Am.*, **74**, pp. 1969-1993 (1984).

26. Raoof, M., Herrmann, R.B. and Malagnini, L. "Attenuation and excitation of three component ground motion in southern California", *Bull. Seism. Soc. Am.*, **89**(4), pp. 888-902 (1999).

27. Roumelioti, Z. and Beresnev, I. "Stochastic finite-fault modeling of ground motions from the 1999 Chi-Chi, Taiwan, earthquake: Application to rock and soil sites with implications for nonlinear site response", *Bull. Seism. Soc. Am.*, **93**(4), pp. 1691-1702 (2003).

28. Malagnini, L. and Hermann, R.B. and Bona, M.D. "Ground-motion scaling in the apennines (Italy)", *Bull. Seism. Soc. Am.*, **90**(4), pp. 1062-1081 (2000).

29. Hatzidimitriou, P.M. "S-wave attenuation in the crust in Northern Greece", *Bull. Seism. Soc. Am.*, **85**(5), pp. 1381-1387 (1995).

30. Chen, S.Z. and Atkinson, G.M. "Global comparisons of earthquake source spectra", *Bull. Seism. Soc. Am.*, **92**(3), pp. 885-895 (2002).

31. Mavroeidis, G.P. and Papageorgiou, A.S. "A mathematical representation of near-fault ground motions", *Bull. Seism. Soc. Am.*, **93**, pp. 1099-1131 (2003).

32. Silva, W. and Darragh, R. "Engineering characterization of strong ground motion recorded at rock sites", *Electric Power Res. Inst. Report TR-102262* (1995).

33. Beresnev, I. and Atkinson, G.M. "Subevent structure of large earthquakes - a ground motion perspective", *Geophys. Res. L.*, **28**, pp. 53-56 (2001).

34. Beresnev, I. and Atkinson, G.M. "Source parameters of earthquakes in Eastern and Western North America based on finite-fault modeling", *Bull. Seism. Soc. Am.*, **92**, pp. 695-710 (2002).

35. Beresnev, I. and Atkinson, G.M. "Generic finite-fault model for ground motion prediction in Eastern North America", *Bull. Seism. Soc. Am.*, **89**, pp. 608-625 (1999).

36. Boore, D.M. and Joyner, W. "Site amplifications for generic rock sites", *Bull. Seism. Soc. Am.*, **87**, pp. 327-341 (1997).

37. Boatwright, J. and Choy, G. "Acceleration source spectra anticipated for large earthquakes in Northeastern North America", *Bull. Seism. Soc. Am.*, **82**, pp. 660-682 (1992).

38. Boore, D.M. "Comparing stochastic point-source and finite-source ground-motion simulations: SMSIM and EXSIM", *Bull. Seism. Soc. Am.*, **99**(6), pp. 3202-3216 (2009).

39. Atkinson, G.M., Assatourians, K., Boore, D.M., Campbell, K. and Motazedian, D. "A guide to differences between stochastic point-source and stochastic finite-fault simulations", *Bull. Seism. Soc. Am.*, **99**(6), pp. 3192-3201 (2009).

BIOGRAPHYIES

Hasan Moghaddam obtained his MS and PhD at Imperial College, London, in the field of Earthquake Engineering, where he also conducted some shaking table tests. At present, he is a faculty member of the civil engineering department of Sharif University of Technology. He has published 16 books, presented over 200 international journal and conference papers and has been invited as lecturer to many international conferences. He has conducted 14 experimental research projects on the seismic behavior of steel connections, FRP strengthening of RC columns, PMS retrofit of RC columns, seismic retrofit of masonry in-filled frames and the seismic strengthening of RC shear walls. He designed the strong floor and shaking-table deck at Sharif University of Technology. As the president of a well known consulting company in Iran (GOMEZ), he has designed and supervised numerous projects on the seismic retrofitting of buildings and industrial structures with some 280,000 m^2 area. He is also engaged in developing national seismic design codes as a member of the relevant scientific committee.

Nader Fanaie obtained his BS, MS and PhD in Civil Engineering at the Department of Civil Engineering in Sharif University of Technology; his MS and PhD theses under the supervision of Professor Moghaddam. He passed several courses at the geophysical institute of Tehran University during his PhD program. He also visited the department of earth sciences at Carleton University taking a sabbatical term. He graduated in 2008 and, at present, is a faculty member of Khajeh Nasir University of Technology. His field of research is signal processing, seismic hazard analysis, seismic hazard deaggregation and earthquake simulation. He has published about 10 journals and conference papers, and also 2 books entitled "Analysis of Structures" and "Strength of Materials" which were

reprinted for the 10th time. He was awarded 3rd rank in the first mathematical competition, held at Sharif University of Technology in 1996, as well as receiving a Gold Medal in "The 4th Iranian Civil Engineering Scientific Olympiad" in 1999. In 2001, he was awarded first ranking in the exam to obtain a PhD scholarship abroad. He was pointed out as an innovative engineer and acknowledged as such on 'Engineering Day' (24 Feb., 2008). He used his scientific experience for two years in his position in the Moshanir Consulting Engineers Co. as Supervisor of a 'Seismic Hazard Analysis' of different power plants in Iran.

Dariush Motazedian obtained his BS in applied Physics in the Physics Department of Shiraz University and was awarded best student in applied physics. His MS was undertaken in the Geophysical Institute of Tehran University and he obtained his PhD in Engineering Seismology under the supervision of Professor Gail Atkinson from Carleton University. At present, he is Associate Professor in the Department of Earth Sciences at Carleton University. In his PhD thesis, he developed a new approach in stochastic modeling, based on dynamic corner frequency, through which observed ground motions are modeled more closely. This approach has been applied successfully to produce a suite of acceleration time series for different regions. His fields of interest are earthquake source modeling, seismic hazard analysis, earthquake signal processing, seismic instrument response calibration and background noise analysis.